Physica Medica 112 (2023) 102619

Contents lists available at ScienceDirect

Physica Medica

journal homepage: www.elsevier.com/locate/ejmp

Enhanced full-inversion-based ultrasound elastography for evaluating tumor response to neoadjuvant chemotherapy in patients with locally advanced breast cancer

Niusha Kheirkhah [a], Anat Kornecki [b], Gregory J. Czarnota [c,d,e], Abbas Samani [a,f,g,h], Ali Sadeghi-Naini [a,c,d,i,*]

[a] School of Biomedical Engineering, Western University, London, ON, Canada
[b] Department of Medical Imaging, Western University, London, ON, Canada
[c] Department of Radiation Oncology, Sunnybrook Health Sciences Centre, Toronto, ON, Canada
[d] Physical Sciences Platform, Sunnybrook Research Institute, Toronto, ON, Canada
[e] Department of Medical Biophysics, University of Toronto, Toronto, ON, Canada
[f] Departments of Medical Biophysics, Western University, London, ON, Canada
[g] Department of Electrical and Computer Engineering, Western University, London, ON, Canada
[h] Imaging Research, Robarts Research Institute, Western University, London, ON, Canada
[i] Department of Electrical Engineering and Computer Science, York University, Toronto, ON, Canada

ARTICLE INFO

Keywords:
Breast cancer
Neoadjuvant chemotherapy
Therapy response monitoring
Tumor stiffness
Elastography
Enhanced strain imaging
Elastic modulus reconstruction

ABSTRACT

Purpose: An enhanced ultrasound elastography technique is proposed for early assessment of locally advanced breast cancer (LABC) response to neoadjuvant chemotherapy (NAC).

Methods: The proposed elastography technique inputs ultrasound radiofrequency data obtained through tissue quasi-static stimulation and adapts a strain refinement algorithm formulated based on fundamental principles of continuum mechanics, coupled with an iterative inverse finite element method to reconstruct the breast Young's modulus (E) images. The technique was explored for therapy response assessment using data acquired from 25 LABC patients before and at weeks 1, 2, and 4 after the NAC initiation (100 scans). The E ratio of tumor to the surrounding tissue was calculated at different scans and compared to the baseline for each patient. Patients' response to NAC was determined many months later using standard clinical and histopathological criteria.

Results: Reconstructed E ratio changes obtained as early as one week after the NAC onset demonstrate very good separation between the two cohorts of responders and non-responders to NAC. Statistically significant differences were observed in the E ratio changes between the two patient cohorts at weeks 1 to 4 after treatment (p-value $<$ 0.001; statistical power greater than 97%). A significant difference in axial strain ratio changes was observed only at week 4 (p-value $=$ 0.01; statistical power $=$ 76%). No significant difference was observed in tumor size changes at weeks 1, 2 or 4.

Conclusion: The proposed elastography technique demonstrates a high potential for chemotherapy response monitoring in LABC patients and superior performance compared to strain imaging.

1. Introduction

Breast cancer is the second most diagnosed cancer in women, estimated to affect 1 in 8 women during their lifetime [1]. About 10–20% of new breast cancer cases are present with locally advanced breast cancer (LABC) [2]. LABC tumors are usually larger than 5 cm and may include varying extent of skin, nipple and/or chest wall involvement and lymphadenopathy [3]. The current standard treatment for LABC includes neoadjuvant chemotherapy (NAC) to shrink the tumor and make it operable before removing it surgically using procedures such as lumpectomy or mastectomy [4]. Several studies have reported a significant correlation between patient response to NAC and improved

* Corresponding author at: Department of Electrical Engineering and Computer Science, Lassonde School of Engineering, York University, LAS 3047, Lassonde Building, 4700 Keele Street, Toronto, ON M3J 1P3, Canada.
E-mail address: asn@yorku.ca (A. Sadeghi-Naini).

https://doi.org/10.1016/j.ejmp.2023.102619
Received 4 March 2022; Received in revised form 15 May 2023; Accepted 5 June 2023
Available online 19 June 2023

treatment outcomes including survival metrics [5–8]. However, complete response is limited to <30% of patients, while about 30–40% of patients do not even partially respond to standard chemotherapy [9–14]. Predicting patient's response early after NAC initiation may enable physicians to offer treatment adjustments (e.g., modifying regimen, dose and/or sequence of treatment options) or even switch to salvage therapy for non-responding patients, before it is too late [15]. Such patient-specific treatment modifications can spare breast cancer patients from unnecessary side effects and improve their overall treatment outcomes and quality of life.

Current approaches for evaluation of response to NAC aim at detecting changes in tumor size in response to treatment [16,17]. They include physical examination or standard anatomical imaging such as mammography, conventional ultrasound imaging, computed tomography (CT) and magnetic resonance imaging (MRI). Tumor size changes, however, may take several months to become detectable, and sometimes may not be evident on imaging despite a favorable histopathological response to therapy [18–20]. As such, these imaging modalities, if being offered to monitor response to NAC, can be effective only a few months after treatment initiation.

In search for more effective monitoring techniques, a number of studies have investigated different functional imaging modalities for evaluating cancer response to treatment [20,21]. Such modalities evaluate physiological, metabolic, and/or molecular changes in the tumor, potentially enabling assessment of therapy response before a change in tumor size is detectable on standard imaging modalities. In this context, dynamic contrast enhanced (DCE) MRI and contrast-enhanced mammography (CEM) have been investigated to detect early changes in tumor physiology as associated with angiogenesis and microcirculation in response to chemotherapy [22–28]. While they showed promise for evaluation of breast cancer response to NAC, both modalities require injection of exogenous contrast agents for each assessment during the course of treatment and DCE-MRI is relatively expensive. Furthermore, tumor response might be associated with fibrosis which often leads to enhancement on contrast imaging modalities, hence not being distinguishable from residual tumor. A number of studies have demonstrated the potential of nuclear medicine imaging including positron emission tomography (PET) for evaluating tumor response to chemotherapy by detecting early changes in tumor metabolism [29,30]. It has been demonstrated that early mean reduction of 2-deoxy-2-[F-18] fluoro-D-glucose (FDG) uptake measured using FDG-PET/CT is significantly higher in responding tumors compared to non-responding lesions [29,30]. PET has also shown potential for early response assessment in breast cancer patients through tumor cell proliferation assessment via quantifying 3′-[F-18] fluoro-3′-deoxythymidine (FLT) uptake [31]. These imaging modalities are, however, not always accessible, often limited in resolution while they need injection of radionuclide contrast agents, limiting the frequency of scanning patients for response evaluation during the course of treatment. Quantitative ultrasound (QUS) is another functional imaging modality that can examine response-related tumor micro-structure characteristics [32–39]. QUS parameters have shown high sensitivity in characterizing tumor cell death in response to cancer therapy in preclinical studies [40,41]. Clinical studies on LABC patients undergoing NAC also demonstrated that early changes in QUS parameters after treatment initiation can differentiate patients in terms of clinical and pathological response and long-term survival [17,42]. Diffuse optical spectroscopic imaging (DOSI) is another possible alternative to other breast imaging modalities. This modality has shown good potential in clinical applications pertinent to breast cancer assessment and diagnosis [43–45]. This method has also been used for monitoring NAC response in patients with breast cancer by probing changes in tumor composition, perfusion, and oxygenation [46–51]. However, the diagnostic performance of DOSI was found to be inferior to that of early metabolic response as monitored by FDG PET/CT in [48]. While DOSI does not require any exogenous contrast agents for imaging, it is associated with long scan time for reconstructing images with acceptable resolution, hence it has not been adapted in the clinic as a standard modality.

Several studies have demonstrated considerable correlation between tumor formation and alteration in tissue biomechanical properties [52–54]. Generally, the dynamic nature of the tissue extracellular matrix (ECM) plays a crucial role in cancer progression [55]. It has been demonstrated that increasing ECM stiffness as a result of excessive collagen generation during tumor formation can directly activates biological processes that result in tumor invasion and metastasis [56]. Moreover, increased collagen content in ECM can promote tumor progression and invasiveness [57–61]. Given that chemotherapy leads to apoptosis and other forms of cell death in tumor, it is anticipated that ECM composition is impacted significantly during effective therapy [62,63]. A manifestation of such alterations is potentially tissue stiffness reduction. In other words, there is a potential correlation between chemotherapy response and tumor softening. In a study conducted by Falou et al., a commercial ultrasound machine was used for clinical strain imaging of breast tumors in 15 LABC patients before and after the start of NAC [64]. Their results demonstrated that changes in relative tumor stiffness can differentiate patients in terms of clinical and pathologic response to treatment as early as 4 weeks after the start of chemotherapy. However, ultrasound strain elastography lacks accuracy in quantifying tissue stiffens as it relies on a poor tissue stress uniformity assumption [65,66]. Recently developed techniques for ultrasound elastography that are capable of quantifying tissue biomechanical properties with precise measures such as Young's modulus can potentially be adapted to monitor the biomechanical alterations in tumor in response to treatment [67,68]. Such methods are anticipated to be capable of more reliable and earlier differentiation between responding and non-responding patients after therapy initiation, compared to strain imaging. Ultrasound elastography is less expensive, potentially more accessible, and is associated with shorter scan times compared to PET, MRI and DOSI. Also, it does not need injection of exogenous contrast agents for imaging.

The present study proposes an enhanced full-inversion-based ultrasound elastography technique to quantify changes in the Young's modulus of LABC tumors as a measure of the response to NAC. This technique applies ultrasound radiofrequency (RF) data acquired via a quasi-static stimulation of breast tissue induced by ultrasound probe. It generates enhanced axial and lateral strain images by enforcing fundamental principles of continuum mechanics [69]. The enhanced strain images are then input to an iterative inverse finite element (FE) algorithm to reconstruct the relative Young's modulus image of the breast tissue [67]. The method was applied to ultrasound RF data acquired from 25 LABC patients undergoing full course of NAC before the treatment (baseline) and at weeks 1, 2, and 4 after the therapy initiation, and its efficacy in chemotherapy response monitoring was investigated.

2. Materials and methods

2.1. Study protocol and data acquisition

This study was conducted in accordance with the institutional research ethics board approval from Sunnybrook Health Sciences Centre, Toronto, Canada. Patients were included in the study based on the following inclusion criteria: age (18–85 years), confirmed diagnosis of LABC, and treatment with NAC followed by surgery. The exclusion criteria for the study involved subjects with inflammatory breast cancer, past medical history of breast abnormalities, significant injury or surgical procedures involving breast, dermatological abnormalities, current or past medical history of connective tissue disease, pregnancy, or lactation. In keeping with the criteria above, twenty-five eligible patients were included in the study after obtaining written informed consent. A core needle biopsy was performed for each patient to confirm cancer diagnosis. Information pertaining to tumor grade, histology, and receptor status was also acquired from respective biopsy specimens. Pre-

and post-treatment MRI were acquired for each patient before the start of NAC and prior to surgery to determine the initial and residual tumor size.

Using a Sonix RP System (Ultrasonix, Vancouver, Canada), ultrasound B-mode images and radiofrequency (RF) data were acquired from the patients' affected breast before treatment as well as at week 1, week 2, and week 4 after the NAC initiation. A 6-cm-wide L14-5/60 transducer operating at a nominal frequency of 10 MHz and a frame rate of 12 frame/s was used in this study. All the ultrasound data were acquired by a trained sonographer following standardized protocols for data acquisition. The patients maintained a supine body position while their arms were placed above their heads throughout the scan. The transducer focus for each patient was determined based on tumor center depth before treatment and it was kept consistent through the rest of the study. On average, 4 scan planes pertaining to different sections of the tumor were acquired for each patient in ~1-cm increments under the guidance of a physician. Raw RF data were acquired at each scan plane before and after a quasi-static stimulation of the breast by the probe while the tumor region contrast was being monitored in the real-time clinical strain image shown by the ultrasound system. The RF data were saved digitally with 16-bit resolution for use in the enhanced elastography method described later.

The patients underwent surgery four to six weeks after completing the course of NAC. The surgical specimens were stained with hematoxylin and eosin (H&E) for histopathology. The histopathology samples were assessed by a board-certified pathologist who was kept blinded to the study results. Patients were categorized into two cohorts of responders and non-responders using the modified response (MR) grading system described in [70,71] that is based on response evaluation criteria in solid tumors (RECIST) [16] and histopathological criteria [19,38]. Patients with a MR score of 1–2 (less than 30% reduction in tumor size) and 3–5 (more than 30% reduction in tumor size or with very low residual tumor cellularity) were determined as non-responders and responders, respectively. In keeping with this, 17 and 8 patients in this study were identified as responders and non-responders, respectively. Table 1 summarizes the clinical characteristics of the patients participated in this study.

Table 1
Participating patients' characteristics.

Characteristics	Mean ± SD/ percentage
Age	51 ± 12 years
Tumor Size (Maximum Diameter)	
Initial Tumor Size	5.42 ± 2.25 cm
Residual Tumor Size	2.25 ± 2.87 cm
Tumor Grade	
I	4%
II	36%
III	60%
Histology	
Invasive Ductal Carcinoma	88%
Invasive Lobular Carcinoma	4%
Invasive Metaplastic Carcinoma	8%
Molecular Features	
ER+	48%
PR+	32%
HER2+	28%
Triple Negative	40%
ER/PR+ & HER2+	16%
ER/PR+ & HER2-	32%
ER&PR- & HER2+	12%
NAC Regimen	
Doxorubicin, Cyclophosphamide, and Paclitaxel (AC-T)	52%
5-Fluorouracil, Epirubicin, cyclophosphamide, and docetaxel (FEC-D)	36%
Docetaxel and Cyclophosphamide (TC)	8%
Adriamycin, Cyclophosphamide, and Docetaxel (AC-D)	4%
Response	
Responders	68%
Non-Responders	32%

2.2. Enhanced strain imaging

Axial and lateral displacement fields for each scan plane were estimated using two frames of ultrasound RF data acquired at two states of tissue pre- and post-mechanical stimulation with the ultrasound probe. In the first step, an initial estimation of the axial and lateral displacement fields was obtained using the method proposed in [72] followed by the Global Ultrasound Elastography (GLUE) method [73]. The resulting fields were then input to the STrain REfinement ALgorithm (STREAL) [69,74,75]. This algorithm improves the accuracy of the displacement fields and strain images by imposing continuum mechanics principles of tissue incompressibility and compatibility through the following steps:

1. Applying Laplacian filtering to smooth the initial displacement fields estimated by GLUE method.
2. Estimating the ratio of out-of-plane strain to axial strain at each point within the tissue computational field of view. This estimate is derived from modeling the breast as semi-infinite medium following the Boussinesq model [75].
3. Enforcing the tissue incompressibility equation in 3D using the estimates obtained in step 2 to refine the axial and lateral displacement fields.
4. Applying the finite difference spatial derivative on the refined displacement fields to generate enhanced images of the tissue axial and lateral strain.
5. Enforcing the strain compatibility equation to further enhance the axial and lateral strain images.

2.3. Full Inversion-Based Young's modulus reconstruction

A full-inversion-based quasi-static elastography technique was adapted to reconstruct relative Young's modulus image of the breast tissue, using the enhanced strain images obtained through the methods presented in the previous section as input [67]. The technique applies iterative algorithm of FE analysis for computing tissue stress distribution resulting from the quasi-static mechanical stimulation followed by Young's modulus (E) calculation using 2D Hooke's law (Equation (1)).

$$\frac{1}{E} = \frac{\varepsilon_{yy}}{\sigma_{yy} - \nu\sigma_{xx}} \tag{1}$$

In this equation, ν is the tissue Poisson's ratio which is set to 0.495 according to breast tissue incompressibility [76,77], and ε and σ represent the strain and stress where the subscripts *yy* and *xx* correspond to the axial and lateral directions, respectively. The iterative process of E reconstruction is stopped when E values of the finite elements stop changing appreciably.

For the stress calculation part of the reconstruction technique, FE analysis was used through ABAQUS FE solver (ABAQUS/Standard, Dassault Systèmes Simulia Corp., Providence, RI, USA). For this analysis, the rectangular field of view of the ultrasound scan plane was meshed using linear quadrilateral elements. In the FE analysis, unlike other techniques that assume ideal unconstrained boundary conditions along the outline of the field of view, we used experimentally measured prescribed displacement boundary conditions along the outline. These displacement boundary conditions were obtained from a subset of the refined displacement data obtained as described earlier, while the high-

quality strain data was used in Equation (1) for updating E in each iteration. Two different methods were used for updating E in each iteration:

1. In the first method, similar to [67], we used Equation (1) throughout the iterations. The relative Young's modulus images obtained from this approach are labelled "axial-strain-based E image".
2. To take advantage of the enhanced lateral strain, we also used Hooke's law in conjunction with the lateral displacements as given in Equation (2). In this method, we used both Eqs. (1) and (2) with weight factors of 10 and 1, respectively, to update E. The relative Youngs' modulus images obtained following this method are labelled "axial/lateral-strain-based E image". The weight factors were selected based on previous reports that estimate the signal-to-noise ratio of ultrasound axial strain images to be typically 10 times higher compared to lateral strain images [78].

$$\frac{1}{E} = \frac{\varepsilon_{xx}}{\sigma_{xx} - \nu\sigma_{yy}} \tag{2}$$

2.4. Data analysis

Using the B-mode images, the region of each tumor was outlined in each scan plane with a physician's guidance. A representative surrounding area of normal tissue was then selected in each scan for calculating the strain or E ratio of the tumor to surrounding normal tissue. At each patient's assessment time, the strain or E ratio was first calculated for each scan plane and then averaged across all scan planes of the tumor to obtain the average ratio for the entire tumor volume. For obtaining the average E value within the tumor area in each scan plane, a Gaussian distribution was fitted to the E values within the tumor region, and the values associated with the lower 30% of the distribution were removed. This pre-processing step was performed to discard small E values pertaining to tumor heterogeneity and to obtain a better estimate of the stiff areas within the tumor region. For calculating the average E value of the surrounding normal tissue in each scan plane, any E value smaller than 50% or larger than 150% of the average E value of the normal tissue region was also discarded following the same argument and the findings of [79] on the mechanical properties of *ex vivo* breast tissue samples. The final E ratio of tumor to normal tissue in each scan plane was then calculated by taking the ratio of the average of the remaining values in each region. A similar method was used to calculate average strain ratios.

Relative changes in the strain and E ratios from the baseline (pre-treatment scan) were calculated for each patient at weeks 1, 2, and 4 after the initiation of NAC. Statistical analysis was conducted using mixed analysis of variance (ANOVA) to assess significance of the difference in strain or E ratio change after NAC between responding and

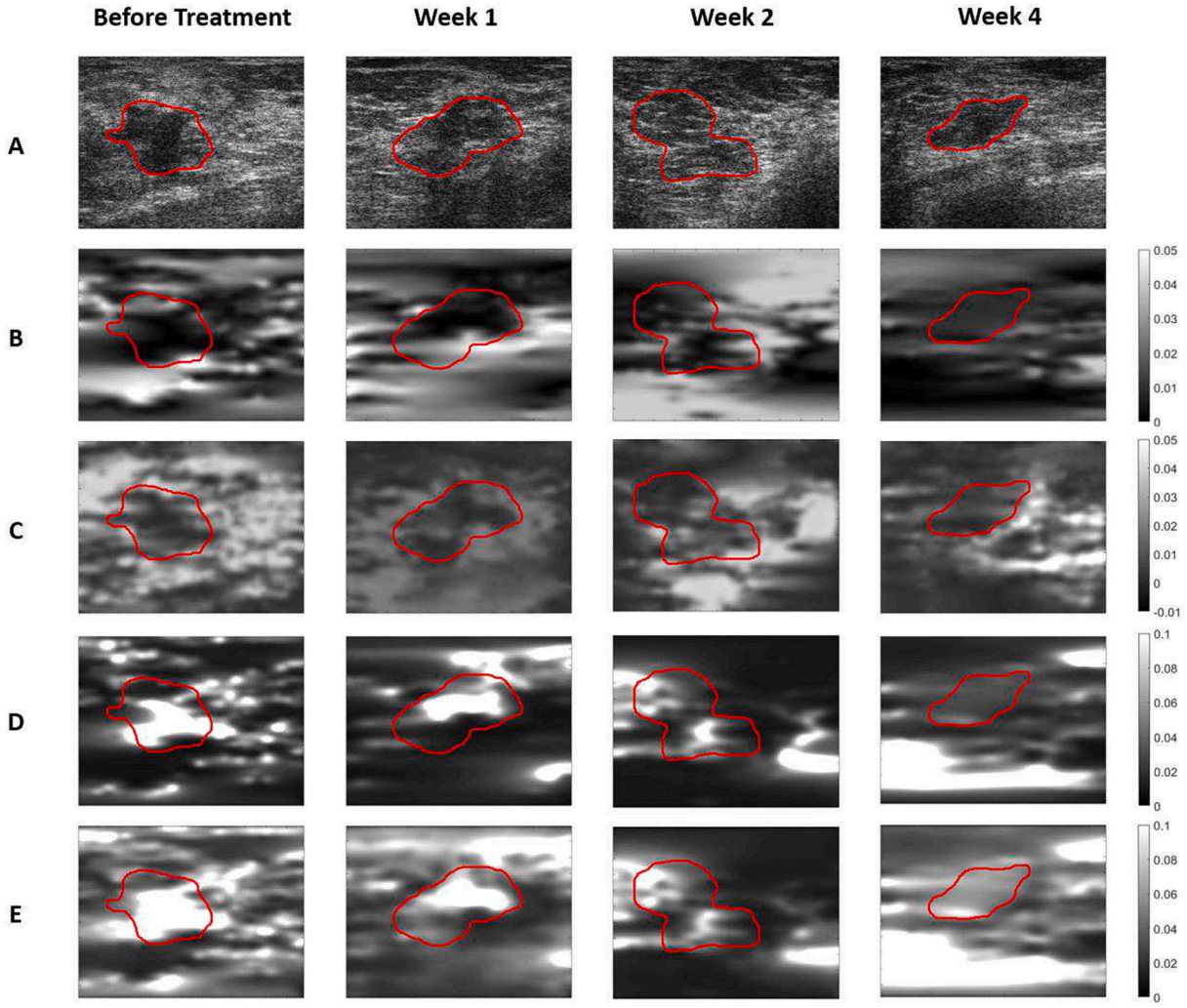

Fig. 1. B-mode (A), axial strain (B), lateral strain (C) and Young's modulus images obtained based on the axial strain (D) and based on axial and lateral strains (E) obtained for a representative responder before and at different times after the NAC initiation. The axial and lateral strain images were generated using the STREAL technique.

non-responding patients. Normality violations in each group of the combination of the two factors (response, scan time) were checked using the Shapiro-Wilk test. A *t*-test (two-sided, 95% confidence) was performed to assess if the two cohorts of patients show any significant difference in the strain or E ratio changes at each scan time (weeks 1, 2, and 4) compared to the baseline. Receiver operating characteristics (ROC) analyses were performed to assess the ability of these parameters at different scan times to differentiate between the response of the two cohorts in terms of the area under the curve (AUC). Similar analyses were performed on tumor size changes from the baseline measured at each scan time using the ultrasound images acquired for each patient.

3. Results

Fig. 1 and Fig. 2 show representative B-mode, strain and E images acquired before and at weeks 1, 2 and 4 after the NAC initiation for a responding and a non-responding patient, respectively. For the responding patient, a continuous reduction in tumor stiffness compared to the baseline is detectable starting from week 1. The reduction is more evident at weeks 2 and 4 after the NAC initiation. For the non-responding patient, minimal changes are observed in tumor stiffness in response to NAC, even at weeks 2 and 4 after the NAC onset. While possible changes in tumor stiffness after NAC can be detected on the strain images, such changes are more evident on the E images. Generally, the axial-strain-based and axial/lateral-strain-based E images have similar quality. However, for some cases the latter show better contrast in identifying tumor and healthy regions. Fig. 3 demonstrate hematoxylin and eosin (H&E) stained histopathology images of the surgical specimens acquired for representative patients. A large residual tumor is observed in the mastectomy specimen of the non-responding patient. The histopathology image of the responding patient demonstrates the tumor bed area with chemotherapy effect and no residual carcinoma. Both images indicate notable heterogeneity within the tumor region.

Estimated from the axial-strain-based E images, the responding (non-responding) patients demonstrated an average tumor-to-normal-tissue E ratio of 3.1 ± 0.7 (3.5 ± 0.8), 2.6 ± 0.8 (3.7 ± 0.6), 2.3 ± 0.7 (3.3 ± 0.9), and 1.7 ± 0.4 (3.2 ± 1.0) at pre-treatment and weeks 1, 2, and 4 after the treatment initiation, respectively. Using the axial/lateral-strain-based E images, an average E ratio of 2.8 ± 0.7 (2.8 ± 0.8), 2.3 ± 0.7 (2.8 ± 0.9), 2.0 ± 0.6 (2.5 ± 1.0), and 1.7 ± 0.4 (2.8 ± 0.9) was estimated for these patients at pre-treatment and weeks 1, 2, and 4 after the start of treatment, respectively. While the average tumor stiffness at the baseline is comparable between the two cohorts, the difference in the average E ratios between the responder and non-responder cohorts shows increases at weeks 1 to 4 after the therapy initiation.

Fig. 4 demonstrates average changes in the strain and E ratios compared to the baseline at different times after NAC initiation for the

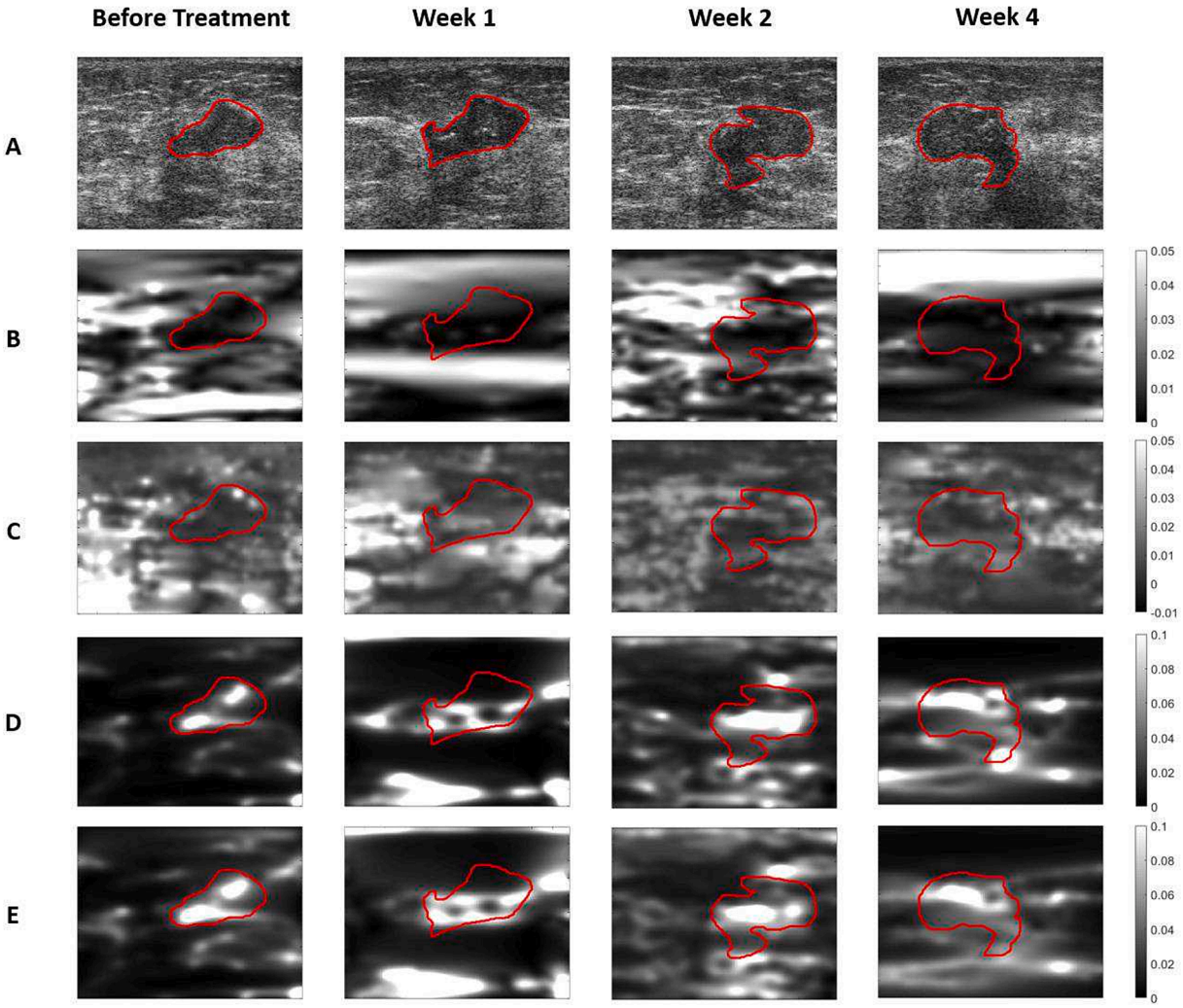

Fig. 2. B-mode (A), axial strain (B), lateral strain (C) and Young's modulus images obtained based on the axial strain (D) and based on axial and lateral strains (E) obtained for a representative non-responder before and at different times after the start of NAC. The axial and lateral strain images were generated using the STREAL technique.

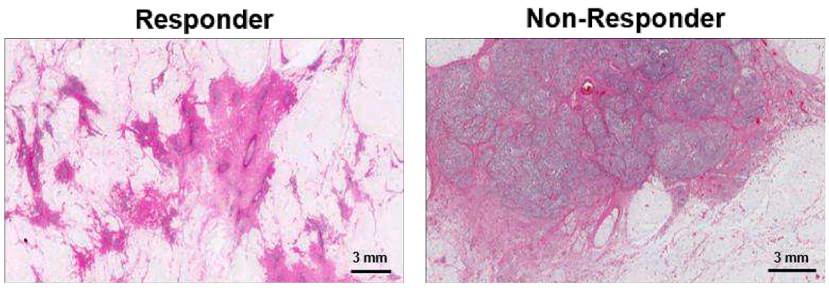

Fig. 3. Histopathology images of surgical specimens obtained from representative responding and non-responding patients.

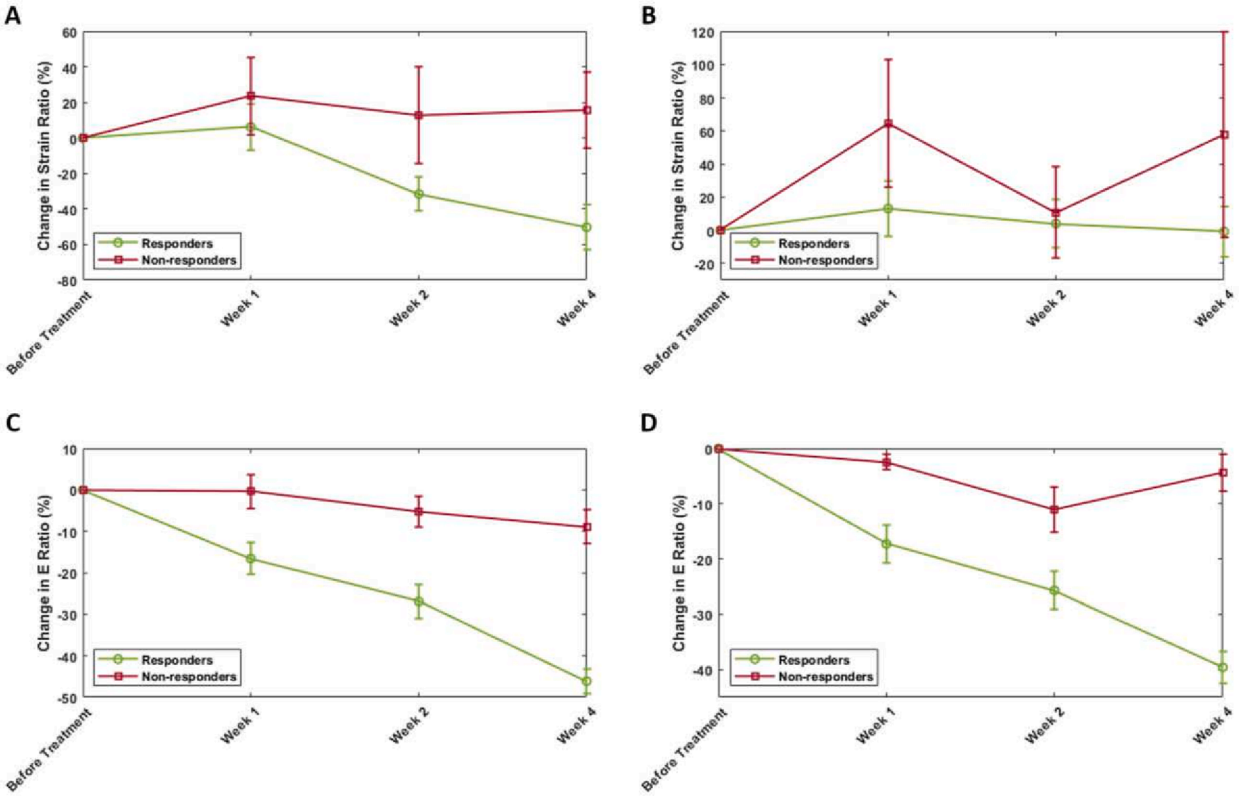

Fig. 4. Relative changes in tumor stiffness compared to baseline after the start of NAC for responding and non-responding patient cohorts, estimated based on axial strain ratio (A), lateral strain ratio (B), E ratio obtained from the axial-strain-based Young's modulus image (C), E ratio obtained from the axial/lateral-strain-based Young's modulus image (D).

two patient cohorts. According to these plots, the axial strain ratio decreases over time after week 1 for the responder cohort while it shows an increase for the non-responder cohort at week 1 with little average changes afterwards. However, the lateral strain ratio demonstrates minimal changes throughout the chemotherapy for the responder cohort while showing elevations for the non-responder cohort. In the plots associated with both versions of the E image, the responder cohort demonstrates a consistent reduction in the average E ratio, starting with 15–20% decrease on average at week 1, followed by 25–30% decrease at week 2 and 40–45% decrease at week 4 following the treatment onset. In contrast, the non-responder cohort shows minimal change in the average E ratio after the start of the chemotherapy with <10% change on average even at week 4 following the treatment initiation. In summary, the change in E ratio for both versions of the E images can completely differentiate responders from non-responders as early as one week after the start of treatment, whereas a clear differentiation cannot be done based on changes in strain ratio until 4 weeks after the NAC initiation. Fig. 5 shows average changes in tumor size from the baseline

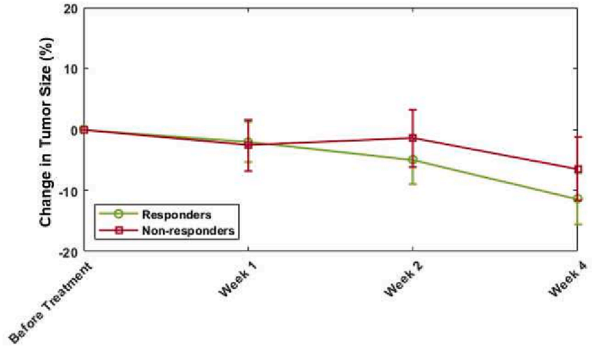

Fig. 5. Relative changes in tumor size compared to baseline after the NAC initiation for responding and non-responding patient cohorts.

at weeks 1, 2 and 4 after the treatment onset. No substantial changes are visible in tumor size to separate the patient cohorts, with ~10% and ~5% average decrease for the responding and non-responding patients at week 4, respectively.

Table 2 shows the results of statistical analysis among the responding and non-responding patients at different scan times. The results obtained from the mixed ANOVA test demonstrate a statistically significant difference in changes in the E ratio between the responding and non-responding patients after the onset of NAC. Such difference is statistically extremely significant in the E ratio changes estimated using both approaches (p-value < 0.001). A similar test conducted for the changes in strain ratios and tumor size demonstrate no significant difference for the lateral strain and tumor size, but an approaching significant difference (p-value $= 0.08$) for the axial strain. The conducted *t*-test demonstrates a statistically significant difference in the E ratio changes from the baseline as early as one week after the treatment onset that is maintained at weeks 2 and 4, with high statistical power. In contrast, no significant difference is observed for changes in the tumor size or lateral strain ratio at weeks 1 to 4. For the axial strain ratio, a significant difference is only seen at week 4 after the treatment initiation. Moreover, results of the ROC analysis demonstrate promising AUCs obtained for changes in the E ratios at weeks 1 to 4 after the start of chemotherapy, and for the axial strain at week 4.

4. Discussion and conclusion

This study investigated, for the first time, the application of a novel full inversion-based ultrasound elastography technique for monitoring tumor response to NAC in LABC patients. The technique adapted the STREAL method [69,74,75] for enhanced strain imaging coupled with a novel methodology for reconstruction of elasticity images that permits accurate quantification of breast tissue relative Young's modulus. The method was applied on ultrasound data acquired from 25 LABC patients before and at weeks 1, 2 and 4 after the NAC initiation. Changes in tumor stiffness in response to NAC was quantified using average E and strain ratios of tumor to surrounding normal tissue obtained at 1, 2 and 4 weeks after the start of NAC initiation. Response of patients to NAC was determined after completing the course of NAC and surgery using the standard clinical and histopathological criteria. The criteria were used for evaluating the performance of the elastography parameters in assessing patients' response to NAC early after the therapy initiation. Trend of changes in tumor Young's modulus among the responding and non-responding patients indicated a very good correlation with the NAC response. In particular, while the tumor E ratio demonstrated a considerable and continuous decrease for responding patients starting at week 1, minimal changes were observed for non-responding patients even at week 4 after the NAC onset.

Estimated from the axial-strain-based and axial/lateral-strain-based E images, the responding versus non-responding patients demonstrated average tumor-to-normal-tissue E ratios of 3.1 ± 0.7 versus 3.5 ± 0.8 and 2.8 ± 0.7 versus 2.8 ± 0.8, respective, before starting the NAC. The estimated average E ratios at the baseline are comparable between the two cohorts and within the range reported for breast cancer in the literature [80]. Statistical analysis confirmed that the method is successful in differentiating responding and non-responding patients as early as one week after the NAC initiation. Specifically, statistically significant differences were observed in E ratio changes between the responding and non-responding patients at all scans after the therapy onset (Table 2). The results of this statistical analysis are indicative of a substantial improvement compared to the previous study in which a significant difference (p-value $= 0.002$) in tumor stiffness changes was only observed after 4 weeks following the start of treatment when such changes were estimated using clinical ultrasound strain imaging [64]. The results obtained in this study with strain images supports the findings of the previous study. Here, a significant difference (p-value $= 0.01$) in changes of the axial strain ratios was observed only at week 4 after the chemotherapy onset. The inferior performance of the strain compared to the E images in early differentiation of the patients' response to NAC can be attributed to the poor stiffness measure of the strain compared to the tissue Young's modulus [66]. Strain image is a true representative of the tissue stiffness only if the stress is uniformity distributed within the breast tissue while being stimulated mechanically with the ultrasound probe for strain-based elastography [65]. Due to the breast tissue inhomogeneity and irregular geometry, and local loading, it is well established that considerable stress non-uniformity exists within the field of view, hindering the sensitivity of strain images in estimating tumor stiffness [67]. The full-inversion-based E reconstruction algorithm applied in this study takes tissue stress non-uniformity into account via finite element analysis, leading to higher signal-to-noise ratio (SNR) in generated E images, hence higher sensitivity in quantifying small changes in tumor stiffness compared to strain images. The statistical analysis on tumor size changes measured using the ultrasound images demonstrated no significant difference between the responding and non-responding patients at weeks 1 to 4 following the treatment initiation. This observation is in agreement with findings of the previous studies in which no statistically significant difference was evident in tumor size changes measured using MRI [81] or ultrasound [82] 3–4 weeks after the start of chemotherapy.

The enhanced axial and lateral strain images obtained using STREAL were utilized to generate two versions of E images. The first version of E images was reconstructed using the enhanced axial images only, while the second version also took advantage of the enhanced lateral strain

Table 2
Results of statistical analysis obtained for different elastography parameters acquired from the responding and non-responding patient cohorts at different times after the NAC initiation. *, †, and ‡ demonstrate statistically significant (p-value < 0.05), highly significant, (p-value < 0.01), and extremely significant (p-value < 0.001), respectively.

Parameter	Week	Mixed ANOVA (p-value)	T-Test (p-value)	Statistical Power	AUC
%ΔTumor-Size	1		0.93	5.1%	0.47
	2	0.90	0.63	8.7%	0.61
	4		0.52	11.2%	0.60
%ΔAxial-Strain-Ratio	1		0.49	10.5%	0.64
	2	0.08	0.17	33.6%	0.74
	4		0.01*	75.8%	0.85
%ΔLateral-Strain-Ratio	1		0.16	23.2%	0.67
	2	0.31	0.82	5.5%	0.51
	4		0.21	15%	0.61
%ΔE-Ratio	1		0.02*	82.8%	0.79
(axial-strain-based E image)	2	<0.001‡	<0.001‡	97.6%	0.85
	4		<0.001‡	99.9%	0.99
%ΔE-Ratio	1		<0.001‡	98.1%	0.82
(axial/lateral-strain-based E image)	2	<0.001‡	0.02*	78.4%	0.77
	4		<0.001‡	99.9%	1.0

images for generating E images with higher quantitative accuracy. The quality of these images was generally comparable, but in some cases the E images reconstructed based on both the axial and lateral strain images led to better visualization of the tumor region compared to those generated based on the axial strain only. Similarly, the trends of changes in the tumor E ratio measured based on these elasticity images were similar over the course of treatment in each response cohort. However, the E ratios associated with the E images generated based on both the axial and lateral strain images provided a relatively better separation between the two cohorts at weeks 1 and 4 after the NAC initiation. In particular, a statistically extremely significant (p-value < 0.001; statistical power $= 98\%$) versus significant (p-value $= 0.02$; statistical power $= 83\%$) difference was observed in the E ratio changes measured at week 1 using the E images reconstructed based on the axial and lateral strain images, and axial strain images, respectively. The results of ROC analysis for both these methods demonstrated a relatively high AUC for NAC response prediction at week 1 after the treatment onset. These observations support the findings of a very recent study in which ultrasound shear wave elastography was applied to measure changes in tumor Young's modulus in breast cancer patients undergoing NAC [82]. In that study, changes in tumor Young's modulus were quantified at weeks 3 and 6 after the NAC initiation, where statistically (highly) significant differences (p-value $= 0.02$ and 0.001) were observed between the patient cohorts with pathological complete versus non-complete response. The findings of this study encourage future studies to investigate the efficacy of the ultrasound shear wave elastography in differentiating the response cohorts at weeks 1 and 2 after the NAC initiation, based on the measured changes in tumor stiffness.

To minimize the effect of mechanical stimulation variations in this study, the tumor stiffness measurements in each scan have been normalized using the surrounding tissue's stiffness measured from the same scan. Furthermore, the study has monitored the relative changes in the stiffness of each tumor at week 1, 2 and 4 after the treatment initiation compared to its baseline (pre-treatment). Therefore, the inter-patient differences between the breast volume and target volume are expected to have minimal effect on this longitudinal analysis.

One limitation associated with this study is the relatively small size of the cohort investigated. The obtained results for the E ratio changes indicate a good level of statistical power for the performed tests. Nevertheless, future studies on larger cohorts are necessary to scrutinize the efficacy of the proposed methods in NAC response monitoring more rigorously. Such investigations can potentially compare the performance of the proposed elastography technique in NAC response prediction with other imaging methods, e.g., QUS, DOSI and MRI, in paired studies. Availability of larger datasets in future studies would also permit adaptation of data-driven models [83] for deep-learning of E images that can lead to improved prediction of therapy response. The responders and non-responder cohorts in this study included similar proportions of grade II and grade III tumors. However, the two cohorts involved fairly different proportions in terms of molecular subtypes of breast cancer. Future studies on larger cohorts can explore whether changes in the measures of tumor stiffness in combination with the molecular features of the disease can improve the differentiation between the responders and non-responders early after the NAC initiation. The majority of the patients in this study received a combination of anthracycline and taxane-based chemotherapy (AC-T: 52%; FEC-D: 36%; AC-D: 4%). The AC-T and FEC-D regimens did not demonstrate any statistically significant difference in E ratio changes measured at week 1, 2, or 4 within the responder cohort (*t*-test, two-sided, 95% confidence). Similarly, the E ratio changes measured for the non-responders at weeks 1 to 4 did not demonstrate any significant difference between these regimens. While the results show no significant intra-group difference in the effect of these NAC regimens on the E ratio changes, future investigations on larger patient populations are required to stratify the participants based on the NAC regimen they received and evaluate the effect of this factor on the study outcome systematically.

In conclusion, this study demonstrated a good potential for the proposed full inversion-based ultrasound elastography technique in assessing and predicating tumor response to NAC in LABC patients as early as one week after the NAC initiation. Early prediction of neo-adjuvant therapy response for these patients can potentially facilitate treatment adjustments by clinicians on an individual patient basis. A personalized paradigm for breast cancer therapeutics is anticipated to improve the overall therapy outcome, survival, and quality of life for the patients. This study, therefore, is a step forward towards precision oncology and tailoring chemotherapies for breast cancer patients. Studies involving larger patient populations are, however, required to further evaluate the efficacy and robustness of the technique, and to compare its performance in NAC response monitoring with other imaging methods.

Declaration of Competing Interest

The authors declare that they have no known competing financial interests or personal relationships that could have appeared to influence the work reported in this paper.

Acknowledgments

This Research was supported by grants from the Natural Sciences and Engineering Research Council (NSERC) of Canada (grant numbers: RGPIN-2016-06472 and RGPIN-2019-06619), the Terry Fox Foundation through a New Frontiers Program Project Grant (grant number: 1083) with funds from the Lotte and John Hecht Memorial Foundation, the Sunnybrook Health Sciences Centre and Western University. A.S.N. holds the York Research Chair in Quantitative Imaging and Smart Biomarkers.

References

[1] Breast cancer statistics | Canadian Cancer Society; 2022. <https://cancer.ca/en/cancer-information/cancer-types/breast/statistics> [accessed May 12, 2023].
[2] Fowble B, Bevan A, Alvarado M, Melisko M. Cancer of the breast. Leibel Phillips Textb Radiat Oncol, Elsevier 2010:1215–323. https://doi.org/10.1016/B978-1-4160-5897-7.00059-7.
[3] Esteva FJ, Hortobagyi GN. Locally advanced breast cancer. Hematol Oncol Clin North Am 1999;13(457–72):vii. https://doi.org/10.1016/s0889-8588(05)70065-4.
[4] Haagensen CD, Stout AP. Carcinoma of the breast. Ann Surg 1943;118:859–70. https://doi.org/10.1097/00000658-194311850-00008.
[5] Fisher B, Bryant J, Wolmark N, Mamounas E, Brown A, Fisher ER, et al. Effect of preoperative chemotherapy on the outcome of women with operable breast cancer. J Clin Oncol 1998;16(8):2672–85.
[6] Cleator SJ, Makris A, Ashley SE, Lal R, Powles TJ. Good clinical response of breast cancers to neoadjuvant chemoendocrine therapy is associated with improved overall survival. Ann Oncol 2005;16:267–72. https://doi.org/10.1093/annonc/mdi049.
[7] Romero A, García-Sáenz JA, Fuentes-Ferrer M, López Garcia-Asenjo JA, Furió V, Román JM, et al. Correlation between response to neoadjuvant chemotherapy and survival in locally advanced breast cancer patients. Ann Oncol 2013;24(3):655–61.
[8] Spring LM, Fell G, Arfe A, Sharma C, Greenup R, Reynolds KL, et al. Pathologic Complete Response after Neoadjuvant Chemotherapy and Impact on Breast Cancer Recurrence and Survival: A Comprehensive Meta-analysis. Clin Cancer Res 2020; 26:2838–48. doi: 10.1158/1078-0432.CCR-19-3492.
[9] Sethi D, Sen R, Parshad S, Khetarpal S, Garg M, Sen J. Histopathologic changes following neoadjuvant chemotherapy in locally advanced breast cancer. Indian J Cancer 2013;50:58–64. https://doi.org/10.4103/0019-509X.112301.
[10] Chuthapisith S, Eremin JM, El-Sheemy M, Eremin O. Neoadjuvant chemotherapy in women with large and locally advanced breast cancer: chemoresistance and prediction of response to drug therapy. Surgeon 2006;4:211–9. https://doi.org/10.1016/S1479-666X(06)80062-4.
[11] Hortobagyi GN. Multidisciplinary management of advanced primary and metastatic breast cancer. Cancer 1994;74:416–23. https://doi.org/10.1002/cncr.2820741329.
[12] Giordano SH. Update on locally advanced breast cancer. Oncologist 2003;8: 521–30. https://doi.org/10.1634/theoncologist.8-6-521.
[13] Haque W, Verma V, Hatch S, Suzanne Klimberg V, Brian Butler E, Teh BS. Response rates and pathologic complete response by breast cancer molecular subtype following neoadjuvant chemotherapy. Breast Cancer Res Treat 2018;170:559–67. https://doi.org/10.1007/s10549-018-4801-3.

[14] Byrski T, Gronwald J, Huzarski T, Grzybowska E, Budryk M, Stawicka M, et al. Pathologic complete response rates in young women with BRCA1-positive breast cancers after neoadjuvant chemotherapy. J Clin Oncol 2010;28(3):375–9.

[15] Huang E, McNeese MD, Strom EA, Perkins GH, Katz A, Hortobagyi GN, et al. Locoregional treatment outcomes for inoperable anthracycline-resistant breast cancer. Int J Radiat Oncol Biol Phys 2002;53(5):1225–33.

[16] Eisenhauer EA, Therasse P, Bogaerts J, Schwartz LH, Sargent D, Ford R, et al. New response evaluation criteria in solid tumours: revised RECIST guideline (version 1.1). Eur J Cancer 2009;45(2):228–47.

[17] Sadeghi-Naini A, Papanicolau N, Falou O, Zubovits J, Dent R, Verma S, et al. Quantitative ultrasound evaluation of tumor cell death response in locally advanced breast cancer patients receiving chemotherapy. Clin Cancer Res 2013;19:2163–74. doi: 10.1158/1078-0432.CCR-12-2965.

[18] Michaelis LC, Ratain MJ. Measuring response in a post-RECIST world: from black and white to shades of grey. Nat Rev Cancer 2006;6:409–14. https://doi.org/10.1038/nrc1883.

[19] Ogston KN, Miller ID, Payne S, Hutcheon AW, Sarkar TK, Smith I, et al. A new histological grading system to assess response of breast cancers to primary chemotherapy: prognostic significance and survival. Breast 2003;12(5):320–7.

[20] Brindle K. New approaches for imaging tumour responses to treatment. Nat Rev Cancer 2008;8:94–107. https://doi.org/10.1038/nrc2289.

[21] Sadeghi-Naini A, Falou O, Hudson JM, Bailey C, Burns PN, Yaffe MJ, et al. Imaging innovations for cancer therapy response monitoring. Imaging Med 2012;4(3):311–27.

[22] Gezer NS, Orbay O, Balci P, Durak MG, Demirkan B, Saydam S. Evaluation of neoadjuvant chemotherapy response with dynamic contrast enhanced breast magnetic resonance imaging in locally advanced invasive breast cancer. J Breast Heal 2014;10:111–8. https://doi.org/10.5152/TJBH.2014.2035.

[23] Sharma A, Sharma S, Sood S, Seam RK, Sharma M, Fotedar V. DCE-MRI and parametric imaging in monitoring response to neoadjuvant chemotherapy in breast carcinoma: a preliminary report. Polish J Radiol 2018;83:e220.

[24] Johansen R, Jensen LR, Rydland J, Goa PE, Kvistad KA, Bathen TF, et al. Predicting survival and early clinical response to primary chemotherapy for patients with locally advanced breast cancer using DCE-MRI. J Magn Reson Imaging 2009;29(6):1300–7.

[25] Wu J, Gong G, Cui Y, Li R. Intratumor partitioning and texture analysis of dynamic contrast-enhanced (DCE)-MRI identifies relevant tumor subregions to predict pathological response of breast cancer to neoadjuvant chemotherapy. J Magn Reson Imaging 2016;44:1107–15. https://doi.org/10.1002/jmri.25279.

[26] Abramson RG, Li X, Hoyt TL, Su P-F, Arlinghaus LR, Wilson KJ, et al. Early assessment of breast cancer response to neoadjuvant chemotherapy by semi-quantitative analysis of high-temporal resolution DCE-MRI: preliminary results. Magn Reson Imaging 2013;31(9):1457–64.

[27] Teruel JR, Heldahl MG, Goa PE, Pickles M, Lundgren S, Bathen TF, et al. Dynamic contrast-enhanced MRI texture analysis for pretreatment prediction of clinical and pathological response to neoadjuvant chemotherapy in patients with locally advanced breast cancer. NMR Biomed 2014;27(8):887–96.

[28] Iotti V, Ravaioli S, Vacondio R, Coriani C, Caffarri S, Sghedoni R, et al. Contrast-enhanced spectral mammography in neoadjuvant chemotherapy monitoring: a comparison with breast magnetic resonance imaging. Breast Cancer Res 2017;19(1). https://doi.org/10.1186/s13058-017-0899-1.

[29] Andrade WP, Lima ENP, Osório CABT, do Socorro Maciel M, Baiocchi G, Bitencourt AGV, et al. Can FDG-PET/CT predict early response to neoadjuvant chemotherapy in breast cancer? Eur J Surg Oncol 2013;39(12):1358–63.

[30] Chuthapisith S, Eremin JM, Eremin O. Predicting response to neoadjuvant chemotherapy in breast cancer: molecular imaging, systemic biomarkers and the cancer metabolome (review). Oncol Rep 2008;20:699–703. https://doi.org/10.3892/or_00000062.

[31] Pio BS, Park CK, Pietras R, Hsueh W-A, Satyamurthy N, Pegram MD, et al. Usefulness of 3'-[F-18]fluoro-3'-deoxythymidine with positron emission tomography in predicting breast cancer response to therapy. Mol Imaging Biol 2006;8(1):36–42.

[32] Oelze ML, O'Brien WD, Zachary JF. Quantitative ultrasound assessment of breast cancer using a multiparameter approach. Proc - IEEE Ultrason Symp 2007:981–4. https://doi.org/10.1109/ULTSYM.2007.250.

[33] Dobruch-Sobczak K, Piotrzkowska-Wróblewska H, Klimoda Z, Secomski W, Karwat P, Markiewicz-Grodzicka E, et al. Monitoring the response to neoadjuvant chemotherapy in patients with breast cancer using ultrasound scattering coefficient: a preliminary report. J Ultrason 2019;19(77):89–97.

[34] Tadayyon H, Sadeghi-Naini A, Wirtzfeld L, Wright FC, Czarnota G. Quantitative ultrasound characterization of locally advanced breast cancer by estimation of its scatterer properties. Med Phys 2014;41(1):012903.

[35] Klimonda Z, Karwat P, Dobruch-Sobczak K, Piotrzkowska-Wróblewska H, Litniewski J. Breast-lesions characterization using Quantitative Ultrasound features of peritumoral tissue. Sci Rep 2019;9:1–9. https://doi.org/10.1038/s41598-019-44376-z.

[36] Sannachi L, Gangeh M, Tadayyon H, Gandhi S, Wright FC, Slodkowska E, et al. Breast cancer treatment response monitoring using quantitative ultrasound and texture analysis: comparative analysis of analytical models. Transl Oncol 2019;12(10):1271–81.

[37] Quiaoit K, DiCenzo D, Fatima K, Bhardwaj D, Sannachi L, Gangeh M, et al. Quantitative ultrasound radiomics for therapy response monitoring in patients with locally advanced breast cancer: Multi-institutional study results. PLoS One 2020;15(7):e0236182.

[38] Tadayyon H, Sannachi L, Gangeh MJ, Kim C, Ghandi S, Trudeau M, et al. A priori prediction of neoadjuvant chemotherapy response and survival in breast cancer patients using quantitative ultrasound. Sci Rep 2017;7(1). https://doi.org/10.1038/srep45733.

[39] Nasief HG, Rosado-Mendez IM, Zagzebski JA, Hall TJ. A quantitative ultrasound-based multi-parameter classifier for breast masses. Ultrasound Med Biol 2019;45:1603–16. https://doi.org/10.1016/j.ultrasmedbio.2019.02.025.

[40] Sadeghi-Naini A, Papanicolau N, Falou O, Tadayyon H, Lee J, Zubovits J, et al. Low-frequency quantitative ultrasound imaging of cell death in vivo. Med Phys 2013;40(8):082901.

[41] Sadeghi-Naini A, Falou O, Tadayyon H, Al-Mahrouki A, Tran W, Papanicolau N, et al. Conventional frequency ultrasonic biomarkers of cancer treatment response in vivo. Transl Oncol 2013;6(3):234–IN2.

[42] Sadeghi-Naini A, Sannachi L, Tadayyon H, Tran WT, Slodkowska E, Trudeau M, et al. Chemotherapy-response monitoring of breast cancer patients using quantitative ultrasound-based intra-tumour heterogeneities. Sci Rep 2017;7(1). https://doi.org/10.1038/s41598-017-09678-0.

[43] Lee K. Optical mammography: diffuse optical imaging of breast cancer. World J Clin Oncol 2011;2:64. https://doi.org/10.5306/wjco.v2.i1.64.

[44] Herranz M, Ruibal A. Optical imaging in breast cancer diagnosis: the next evolution. J Oncol 2012;2012:1–10.

[45] Applegate MB, Istfan RE, Spink S, Tank A, Roblyer D. Recent advances in high speed diffuse optical imaging in biomedicine. APL Photonics 2020;5:40802. https://doi.org/10.1063/1.5139647.

[46] Gunther JE, Lim EA, Kim HK, Flexman M, Altoé M, Campbell JA, et al. Dynamic diffuse optical tomography for monitoring neoadjuvant chemotherapy in patients with breast cancer. Radiology 2018;287(3):778–86.

[47] Schaafsma BE, Van De Giessen M, Charehbili A, Smit VTHBM, Kroep JR, Lelieveldt BPF, et al. Optical mammography using diffuse optical spectroscopy for monitoring tumor response to neoadjuvant chemotherapy in women with locally advanced breast cancer. Clin Cancer Res 2015;21:577–84. doi: 10.1158/1078-0432.CCR-14-0736.

[48] Ueda S, Yoshizawa N, Shigekawa T, Takeuchi H, Ogura H, Osaki A, et al. Near-infrared diffuse optical imaging for early prediction of breast cancer response to neoadjuvant chemotherapy: a comparative study using 18F-FDG PET/CT. J Nucl Med 2016;57(8):1189–95.

[49] Falou O, Soliman H, Sadeghi-Naini A, Iradji S, Lemon-Wong S, Zubovits J, et al. Diffuse optical spectroscopy evaluation of treatment response in women with locally advanced breast cancer receiving neoadjuvant chemotherapy. Transl Oncol 2012;5(4):238–46.

[50] Liu YH, Xue LB, Yang YF, Zhao TJ, Bai Y, Zhang BY, et al. Diffuse optical spectroscopy for monitoring the responses of patients with breast cancer to neoadjuvant chemotherapy. Medicine (Baltimore) 2018;97(41):e12683.

[51] Zhi W, Liu G, Chang C, Miao A, Zhu X, Xie Li, et al. Predicting treatment response of breast cancer to neoadjuvant chemotherapy using ultrasound-guided diffuse optical tomography. Transl Oncol 2018;11(1):56–64.

[52] Runel G, Lopez-Ramirez N, Chlasta J, Masse I. Biomechanical properties of cancer cells. Cells 2021;10(4):887.

[53] Deville SS, Cordes N. The extracellular, cellular, and nuclear stiffness, a trinity in the cancer resistome—a review. Front Oncol 2019;9:1376. https://doi.org/10.3389/FONC.2019.01376/BIBTEX.

[54] Broders-Bondon F, Ho-Bouldoires THN, Fernandez-Sanchez ME, Farge E. Mechanotransduction in tumor progression: the dark side of the force. J Cell Biol 2018;217:1571–87. https://doi.org/10.1083/JCB.201701039.

[55] Cox TR, Erler JT. Remodeling and homeostasis of the extracellular matrix: Implications for fibrotic diseases and cancer. DMM Dis Model Mech 2011;4:165–78. https://doi.org/10.1242/dmm.004077.

[56] Wei SC, Fattet L, Tsai JH, Guo Y, Pai VH, Majeski HE, et al. Matrix stiffness drives epithelial-mesenchymal transition and tumour metastasis through a TWIST1-G3BP2 mechanotransduction pathway. Nat Cell Biol 2015;17(5):678–88.

[57] Jena MK, Janjanam J. Role of extracellular matrix in breast cancer development: a brief update. F1000Res 2018;7:274.

[58] Walker C, Mojares E, del Río Hernández A. Role of extracellular matrix in development and cancer progression. Int J Mol Sci 2018;19(10):3028.

[59] Xu S, Xu H, Wang W, Li S, Li H, Li T, et al. The role of collagen in cancer: from bench to bedside. J Transl Med 2019;17(1). https://doi.org/10.1186/S12967-019-2058-1.

[60] Winkler J, Abisoye-Ogunniyan A, Metcalf KJ, Werb Z. Concepts of extracellular matrix remodelling in tumour progression and metastasis. Nat Commun 2020.1–19.;2020(111):11. https://doi.org/10.1038/s41467-020-18794-x.

[61] Armstrong T, Packham G, Murphy LB, Bateman AC, Conti JA, Fine DR, et al. Type I collagen promotes the malignant phenotype of pancreatic ductal adenocarcinoma. Clin Cancer Res 2004;10:7427–37. doi: 10.1158/1078-0432.CCR-03-0825.

[62] Gonzalez-Molina J, Moyano-Galceran L, Single A, Gultekin O, Alsalhi S, Lehti K. Chemotherapy as a regulator of extracellular matrix-cell communication: implications in therapy resistance. Semin Cancer Biol 2022;86:224–36. https://doi.org/10.1016/j.semcancer.2022.03.012.

[63] Fatherree JP, Guarin JR, McGinn RA, Naber SP, Oudin MJ. Chemotherapy-induced collagen IV drives cancer cell motility through activation of src and focal adhesion kinase. Cancer Res 2022;82:2031–44. doi: 10.1158/0008-5472.CAN-21-1823.

[64] Falou O, Sadeghi-Naini A, Prematilake S, Sofroni E, Papanicolau N, Iradji S, et al. Evaluation of neoadjuvant chemotherapy response in women with locally advanced breast cancer using ultrasound elastography. Transl Oncol 2013;6(1):17–24.

[65] Sigrist RMS, Liau J, El KA, Chammas MC, Willmann JK. Ultrasound elastography: review of techniques and clinical applications. Theranostics 2017;7:1303–29. https://doi.org/10.7150/thno.18650.

[66] Mousavi SR, Sadeghi-Naini A, Czarnota GJ, Samani A. Towards clinical prostate ultrasound elastography using full inversion approach. Med Phys 2014;41(3):033501.
[67] Mousavi SR, Rivaz H, Sadeghi-Naini A, Czarnota GJ, Samani A. Breast ultrasound elastography using full inversion-based elastic modulus reconstruction. IEEE Trans Comput Imaging 2017;3:774–82. https://doi.org/10.1109/TCI.2017.2741422.
[68] Mousavi SR, Rivaz H, Czarnota GJ, Samani A, Sadeghi-Naini A. Ultrasound elastography of the prostate using an unconstrained modulus reconstruction technique: a pilot clinical study. Transl Oncol 2017;10:744–51. https://doi.org/10.1016/j.tranon.2017.06.006.
[69] Kheirkhah N, Dempsey S, Sadeghi-Naini A, Samani A. A novel tissue mechanics-based method for improved motion tracking in quasi-static ultrasound elastography. Med Phys 2023;50(4):2176–94.
[70] Tadayyon H, Gangeh M, Sannachi L, Trudeau M, Pritchard K, Ghandi S, et al. *A priori* prediction of breast tumour response to chemotherapy using quantitative ultrasound imaging and artificial neural networks. Oncotarget 2019;10(39):3910–23.
[71] Moghadas-Dastjerdi H, Sha-E-Tallat HR, Sannachi L, Sadeghi-Naini A, Czarnota GJ. A priori prediction of tumour response to neoadjuvant chemotherapy in breast cancer patients using quantitative CT and machine learning. Sci Reports 2020 101 2020;10:1–11. doi: 10.1038/s41598-020-67823-8.
[72] Rivaz H, Boctor EM, Choti MA, Hager GD. Real-time regularized ultrasound elastography. IEEE Trans Med Imaging 2011;30:928–45. https://doi.org/10.1109/TMI.2010.2091966.
[73] Hashemi HS, Rivaz H. Global time-delay estimation in ultrasound elastography. IEEE Trans Ultrason Ferroelectr Freq Control 2017;64:1625–36. https://doi.org/10.1109/TUFFC.2017.2717933.
[74] Kheirkhah N, Dempsey SCH, Rivaz H, Samani A, Sadeghi-Naini A. A tissue mechanics based method to improve tissue displacement estimation in ultrasound elastography. In: 42nd annu int conf IEEE eng med biol soc, Montreal, QC, Canada; 2020. p. 2051–4. doi: 10.1109/EMBC44109.2020.9175869.
[75] Kheirkhah N, Sadeghi-Naini A, Samani A. Analytical estimation of out-of-plane strain in ultrasound elastography to improve axial and lateral displacement fields. 42nd Annu Int Conf IEEE Eng Med Biol Soc 2020:2055–8. https://doi.org/10.1109/EMBC44109.2020.9176086.
[76] Ramião NG, Martins PS, Rynkevic R, Fernandes AA, Barroso M, Santos DC. Biomechanical properties of breast tissue, a state-of-the-art review. Biomech Model Mechanobiol 2016;15:1307–23. https://doi.org/10.1007/s10237-016-0763-8.
[77] Plewes DB, Bishop J, Samani A, Sciarretta J. Visualization and quantification of breast cancer biomechanical properties with magnetic resonance elastography. Phys Med Biol 2000;45:1591–610. https://doi.org/10.1088/0031-9155/45/6/314.
[78] Szabo TL. Diagnostic ultrasound imaging: inside out, 2nd ed. Elsevier Inc.; 2004. doi: 10.1016/C2011-0-07261-7.
[79] Dempsey SCH, O'Hagan JJ, Samani A. Measurement of the hyperelastic properties of 72 normal homogeneous and heterogeneous ex vivo breast tissue samples. J Mech Behav Biomed Mater 2021:124. https://doi.org/10.1016/J.JMBBM.2021.104794.
[80] Samani A, Zubovits J, Plewes D. Elastic moduli of normal and pathological human breast tissues: an inversion-technique-based investigation of 169 samples. Phys Med Biol 2007;52:1565–76. https://doi.org/10.1088/0031-9155/52/6/002.
[81] Pereira NP, Curi C, Osório CABT, Marques EF, Makdissi FB, Pinker K, et al. Diffusion-weighted magnetic resonance imaging of patients with breast cancer following neoadjuvant chemotherapy provides early prediction of pathological response – a prospective study. Sci Rep 2019;9:1–8. https://doi.org/10.1038/s41598-019-52785-3.
[82] Gu J-H, He C, Zhao Q-Y, Jiang T-A. Usefulness of new shear wave elastography in early predicting the efficacy of neoadjuvant chemotherapy for patients with breast cancer: where and when to measure is optimal? Breast Cancer 2022;29(3):478–86.
[83] Sirjani N, Ghelich Oghli M, Kazem Tarzamni M, Gity M, Shabanzadeh A, Ghaderi P, et al. A novel deep learning model for breast lesion classification using ultrasound Images: a multicenter data evaluation. Phys Medica 2023;107:102560.